Microtubule seams are not mechanically weak defects

Brandon J. Harris,[1,2] Jennifer L. Ross,[3] and Taviare L. Hawkins[2]
[1]*Biology Department, University of Wisconsin–La Crosse, La Crosse, Wisconsin 54601, USA*
[2]*Department of Physics, University of Wisconsin–La Crosse, La Crosse, Wisconsin 54601, USA*
[3]*Department of Physics, University of Massachusetts Amherst, Amherst, Massachusetts 01003, USA*

(Received 20 February 2018; published 14 June 2018)

Microtubule rigidity is important for many cellular functions to support extended structures and rearrange materials within the cell. The arrangement of the tubulin dimers within the microtubule can be altered to affect the protofilament number and the lattice type. Prior electron microscopy measurements have shown that when polymerized in the presence of a high concentration of NaCl, microtubules were more likely to be ten protofilaments with altered intertubulin lattice types. Specifically, such high-salt microtubules have a higher percentage of seam defects. Such seams have long been speculated to be a mechanically weak location in the microtubule lattice, yet no experimental evidence supported this claim. We directly measured the persistence length of freely fluctuating filaments made either with high salt or without. We found that the microtubules made with high salt were more flexible, by a factor of 2, compared to those polymerized the same way without salt present. The reduced persistence length of the high-salt microtubules can be accounted for entirely by a smaller cross-sectional radius of these microtubules, implying that the mixed lattice interactions have little effect on the bending rigidity. Our results suggest that the microtubule seam is not weaker than the typical lattice structure as previously speculated from structural studies.

DOI: 10.1103/PhysRevE.97.062408

I. INTRODUCTION

Tubulin dimers composed of alpha and beta tubulin monomers are the building blocks of microtubule filaments in cells [Fig. 1(a)]. They polymerize through entropically driven self-assembly. Tubulin dimers can attach to each other through electrostatic and hydrophobic interactions to form a variety of structures including tubes, rings, and sheets [1].

Cellular microtubules have 13 protofilaments that run parallel to the long axis [Fig. 1(b)]. The lateral binding is often between tubulin proteins of the same type (alpha to alpha, beta to beta), and this is called a B lattice [2]. Because of the natural pitch of the B lattice, the microtubule cylinder closes at a location where the B lattice is shifted by three monomers (3-start helix) and mismatched (alpha-to-beta). This mismatch defect is called the seam [3]. An A lattice is when an entire microtubule is made from alternating alpha-beta lateral interactions. Cellular microtubules of cilia have been shown to display an A lattice [2]. It is unknown if the A lattice tubulin interactions are inherently weaker or stronger than the B lattice interactions.

Structural studies of microtubules first identified the seam as a defect in the closed lattice when microtubules were reconstituted *in vitro* [4]. The same seams were also visualized in live cells [3]. Several structural studies have speculated that the seam is likely a weak interaction site in the filament structure [5–7], yet no direct experimental work has produced evidence to support or reject this speculation. Here, we directly probe the mechanical properties of microtubules that have a high number of seams along their entire length.

We can make microtubules with a high percentage (∼50%) of seam defects by polymerizing them in the presence of 580 m*M* NaCl. Prior work, using electron microscopy, showed that such "high-salt" microtubules polymerize into tubes, but have mostly ten protofilaments and a mixed lattice type with numerous seam defects [8,9] [Fig. 1(d)]. These microtubules give the opportunity to determine if the microtubule seam has different interaction energies that might affect microtubule rigidity.

The flexural rigidity of a filament is a measure of the bending stiffness. It depends on both the Young's (bending) modulus, E, and the second moment of the cross-sectional area of the object, I. For biopolymers, we often use the persistence length of the filament to refer to the bending rigidity. The persistence length is the length scale over which a fluctuating filament's tangential angle becomes decorrelated; this is proportional to the flexural rigidity:

$$L_p = \frac{EI}{k_B T}, \tag{1}$$

At the microscopic level, the Young's modulus, a continuum mechanical property of the microtubules, should depend on the interaction energies between the dimers [10,11]. The high-salt microtubules with their mixed A and B lattices could have altered interaction energies compared to standard microtubules with predominantly B lattices. Additionally, because the rigidity also depends on the cross section of the microtubule, high-salt microtubules are expected to have altered persistence lengths compared to typical microtubules.

Taken together, high-salt microtubules offer a unique structure to investigate the relative contributions of the lattice interactions and the number of protofilaments to the overall stiffness of the filament. Here, we report the persistence length of microtubules made with and without high concentrations of NaCl. We find that high-salt microtubules have a persistence

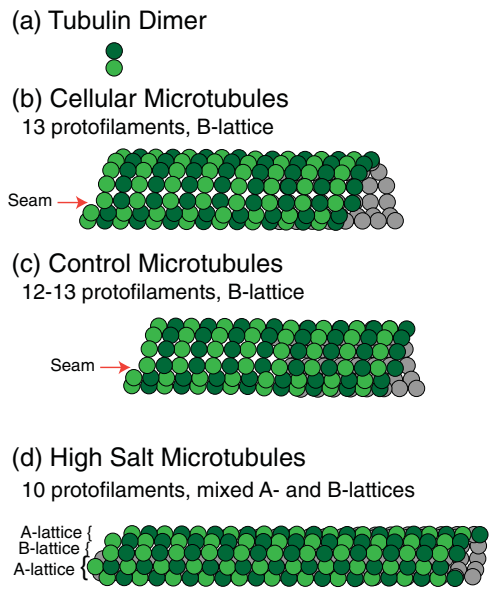

FIG. 1. Cartoon schematics of microtubule structures. (a) The tubulin dimer is made from an alpha tubulin (light green) and beta tubulin (dark green). (b) Cellular microtubules are comprised of 13 protofilaments and have a B lattice with a single A lattice seam defect (red arrow). (c) Control microtubules are similar to cellular microtubules but with 12 or 13 protofilaments. (d) High-salt microtubules are typically nine or ten protofilaments and display a mixed A lattice and B lattice.

length which is half that of microtubules polymerized without high salt (control). Using the known structure of both types of microtubules, we can deduce the ratio of the bending moduli of the high-salt and the control microtubules. We find that the lattice type has no detectable effect on the bending modulus within the experimental uncertainty of our measurements. Our results support a model where the seam is not a weak point in the lattice.

II. METHODS

A. Microtubule polymerization

All reagents were purchased from Sigma-Aldrich (St. Louis, MO) unless otherwise stated. Both labeled and unlabeled tubulin from porcine brain was purchased from Cytoskeleton, Inc. (Denver, CO) in lyophilized form and stored in –80 °C. Tubulin was resuspended to a concentration of 5 mg mL^{-1} using PEM-100 (100 mM Na-PIPES, 1 mM $MgSO_4$, 1 mM EGTA, pH 6.8) for 10 min on ice. Rhodamine tubulin was mixed with unlabeled tubulin to produce a 1:5 labeled:total tubulin dimer ratio. To remove aggregated tubulin dimers, the tubulin mixture was centrifuged at 360 000× g at 4 °C for 20 min. To polymerize control microtubules, 1 mM of GTP was added to tubulin dimers. For high-salt microtubules, 1 mM GTP and 580 mM NaCl (Acros Organics, NJ) were added to tubulin dimers. Both sets of tubulin were polymerized by incubating at 37 °C for 20 min, stabilized by the addition of 50 μM paclitaxel (Taxol), and equilibrated by incubating at 37 °C for 20 min. Microtubules were centrifuged at 25 °C for 10 min to remove unpolymerized tubulin. Microtubules were resuspended in the original volumes of PEM-100 with 50 μM Taxol.

B. Microscopy setup and acquisition specifications

Sample preparation for microscopy was described previously [12,13]. Briefly, microtubules were diluted to 0.45 μM in PEM-100 with 50 μM Taxol. A small volume (1 – 3 μl) was pipetted onto a slide and closed with a 22 × 22 mm^2 cover glass. The small volume spread throughout the cover glass area to make a thin sample that is approximately 2 – 6 μm thick. Fluorescent microtubules were imaged using epifluorescence microscopy suited for rhodamine dye (excitation 520–540 nm, emission 580–600 nm). A Nikon Ti-U model microscope with a 60×, 1.49 NA, oil immersion objective, Chroma 96364 ET-DsRed filter cube, Andor iXon3 EMCCD camera (Model No. DU-897E-CSO-#BV), and NIS-Elements AR software (ver. 4.50.00) were used for data acquisition. A 0.27 μm/pixel calibration, 200 ms exposure rate, 300 electron multiplying (EM) gain, 10 MHz readout speed, and 5.1× conversion gain were used as settings for all images acquired. Each individual microtubule was captured for 500 individual sequential frames and saved as a TIF image sequence.

C. Image processing and statistical analysis

We have previously extensively described the method we employ to perform image analysis to extract the persistence length measurement [12,13]. We refer the reader to those publications for specifics on the analysis. This technique was established independently by two groups [14,15], and has been used many times by a large number of groups previously [12,13,16–23]. Each TIF image sequence was imported into FIJI, a package version of IMAGEJ [24]. The brightness and contrast were autoadjusted, and the background was normalized. The image was converted to binary and skeletonized using the skeletonize plug-in in FIJI. Skeletonized image sequences were used for MATLAB (MathWorks, ver. R2017A, Natick, MA) analysis of the normal modes to determine persistence length. The measurement uses the variance of the normal mode amplitudes to determine the mechanical properties of the microtubules. We added an extra step to the method to use bootstrapping to resample the data to find the uncertainty of the variance measurement [12]. Bootstrapping statistics were performed using R [25] as previously described [12].

To compare raw data sets of persistence length measurements, we used an online application that performs a Kolmogorov-Smirnov test (KS test) [26]. Comparisons between normal distributions were compared using the Student's t test in KALEIDAGRAPH (Synergy Software, Reading, PA).

III. RESULTS AND DISCUSSION

We polymerized two sets of microtubules at the same time from the same tubulin batch. One set had 580 mM NaCl in the buffer during polymerization (high salt), and the other was polymerized without additional NaCl (control). Both sets of microtubules were stabilized with Taxol, a chemotherapeutic drug, present at the same concentration.

We imaged the microtubule filaments in a thin chamber, 3 μm in thickness, so that they would stay focused in the

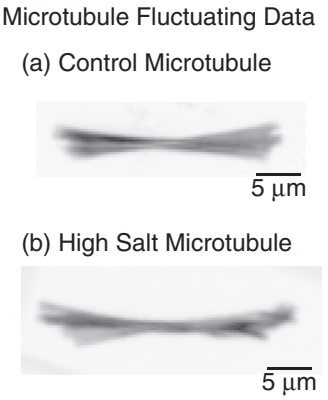

FIG. 2. Microtubule fluctuations. Example overlays of multiple images of a fluctuating filament from (a) control and (b) high-salt microtubules. Scale bar is 5 μm.

z direction of the imaging field. An overlay of a filament's shape over time visually verified fluctuations primarily in the xy plane (Fig. 2). It is important to note that freely fluctuating filaments can also diffuse and rotate in the chamber; they have free boundary conditions. Using the same preparation method, we have recently compared control microtubules that are freely fluctuating or bound on one end, and have found no statistical difference in the measured persistence lengths [21].

In the current experiment, we measured the persistence lengths and contour lengths of each microtubule. The microtubules we imaged had contour lengths ranging from 5 to 35 μm. Plotting the persistence length as a function of contour length, we see no length dependence (Fig. 3). This is as we have previously reported [12,13,21]. Only two groups have reported a length-dependent persistence length [19,27], with the most surprising and strikingly large length dependence shown by Pampaloni *et al.* [27]. Many other studies before and since that time have been published and no other has shown length

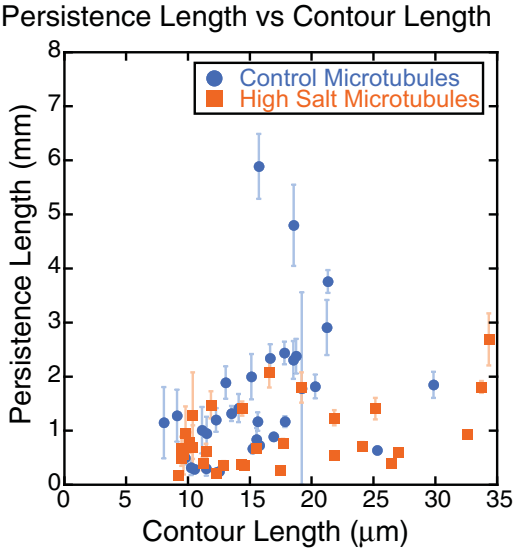

FIG. 3. The persistence length as a function of contour length for control (blue circles, $N = 33$) and high-salt (orange squares, $N = 30$) microtubules.

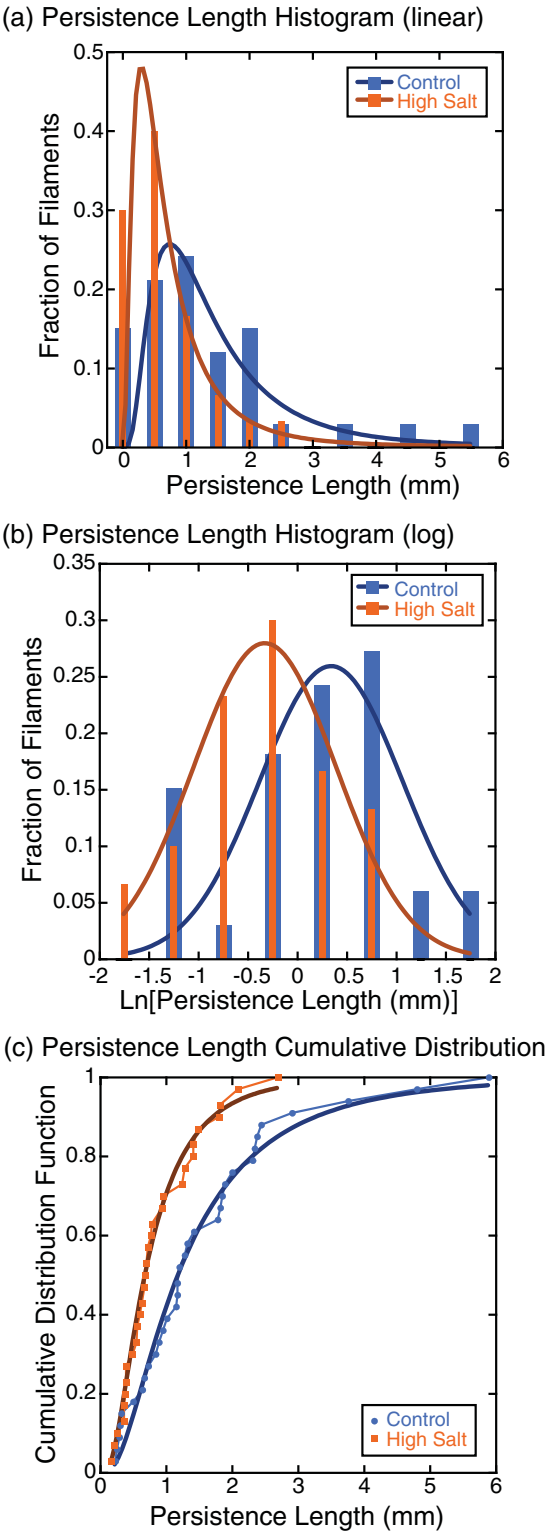

FIG. 4. Distributions of persistence length measurements. (a) Probability distribution with a bin size of 0.5 mm for control (blue bars, $N = 33$) and high-salt (orange bars, $N = 30$) microtubules fit to Eq. (2). (b) Probability distribution of the log of the persistence length with a bin size of 0.5 for control (blue bars) and high-salt (orange bars) fit to a Gaussian function given in Eq. (3). (c) Cumulative distribution of control (blue circles) and high-salt (orange squares) fit to Eq. (4). Fit parameters are in given in Tables I–III.

dependence at similar contour lengths [11–13,16,21–23,28]. One difference between our technique and that employed by groups observing a length-dependent persistence length is that our filaments have free boundary conditions and the other groups have microtubules affixed to one end. In a recent publication, we used the exact same set of microtubules in both freely fluctuating and single-end affixed geometries and found no difference in the persistence length nor was there a dependence on the contour length [21]. Further, other recent work using similar measurements with filaments affixed to one end did not report length-dependent measurements [29]. From this evidence, our data, with the majority of other data in the field, support the conclusion that microtubule persistence length is independent of contour length.

Examining the probability distribution functions (PDFs) of persistence lengths for both high-salt and control microtubules, we find that they are lognormally distributed [Fig. 4(a)]. The lognormal distribution has been observed in several prior studies measuring microtubule persistence length [12–14,20,21,23]. We previously discussed that lognormal distributions often arise when the quantity is a product of independent variables with similar widths. The persistence length is a product of the Young's modulus, E, and the second moment of area, I [Eq. (1)], both of which could be normally distributed.

For lognormal PDFs, there are several ways to examine and analyze the data. First, we fit the data to a lognormal function of the form

$$f(x) = \left(\frac{A}{x\sigma}\right) e^{\left(\frac{[\ln(x)-\mu]^2}{2\sigma^2}\right)}, \tag{2}$$

where A is an amplitude, σ is the width parameter for the $\mathrm{Ln}(x)$, and μ is the position parameter for the $\mathrm{Ln}(x)$, where the exponential of μ is the median of the distribution. Using the fit parameter, μ, and taking the exponential of that value, we can calculate the median of the persistence length distribution to find 1.2 ± 0.5 mm ($R^2 = 0.64$) for control and 0.6 ± 1.4 mm ($R^2 = 0.55$) for the high-salt microtubules. Performing a Kolmogorov-Smirnov statistical test (KS test) of the data, we find that the probability that these two distributions are the same is only 0.8% ($p = 0.008$). Thus, the high-salt microtubules have a distinct persistence length from control microtubules. Unfortunately, the uncertainties on the fit parameters are relatively high (Table I).

In order to fit the data better and to be able to compare with standard statistical tests, we need to use normally distributed data. For lognormal data, we can take the natural log of each measurement, bin the data to create a PDF of the log-transformed data, and fit it to a Gaussian [Fig. 4(b)]:

$$f(x) = Ae^{-\frac{(x-x_0)^2}{2\delta^2}}, \tag{3}$$

TABLE I. Probability distribution fits to lognormal distribution [Eq. (2)].

	A	μ	σ	R^2	L_p (mm)
Control	0.17 ± 0.04	0.2 ± 0.2	0.7 ± 0.2	0.64	1.2 ± 0.5
High salt	0.2 ± 0.2	-0.5 ± 1.0	0.8 ± 1	0.55	0.6 ± 1.4

TABLE II. Probability distribution fits for logarithmically rescaled data [Eq. (3)].

	A	x_0	δ	R^2	L_p (mm)
Control	0.25 ± 0.06	0.3 ± 0.2	0.7 ± 0.2	0.64	1.4 ± 0.5
High salt	0.27 ± 0.03	-0.32 ± 0.08	0.7 ± 0.07	0.92	0.7 ± 0.1

where A is the amplitude, x_0 is the mean value, and δ is the standard deviation. The mean value of the PDF of the log data reflects the median of the persistence lengths: 1.4 ± 0.5 mm for control ($R^2 = 0.64$) and 0.7 ± 0.1 mm for high-salt microtubules ($R^2 = 0.93$). Because these PDFs are normally distributed, we can use the Student's t test to compare the data, and find the probability that they are the same is 1% ($p = 0.01$). All the fit information can be found in Table II.

Lastly, all the data can be displayed using a cumulative distribution function (CDF) instead of binning the data. The cumulative distribution of a lognormal has the form

$$f(x) = 0.5\left\{1 + \mathrm{erf}\left[\frac{\ln(x) - \mu}{\sqrt{2}\sigma}\right]\right\}, \tag{4}$$

where μ is the natural log of the median and σ is the standard deviation of the natural log of the distribution. Using Eq. (4), we find the median to be 1.19 ± 0.04 mm for control ($R^2 = 0.98$) and 0.69 ± 0.02 mm for the high salt ($R^2 = 0.99$). The fit parameters can be found in Table III.

Interestingly, all fits to the data give the average persistence length of the control microtubules to be about 1.2 mm, which is similar to prior work for the same types of microtubules [12,13]. In this prior work, our reported persistence lengths were reduced by a factor of 2 due to our method of segmentation of the filaments. After correcting this effect, we found that our prior reported persistence lengths should be larger by exactly a factor of 2, making our current and prior measurements identical.

Comparing the characteristic persistence lengths from the data represented three different ways, we find that the PDF data fits [Eqs. (2) and (3)] are each with significantly higher uncertainty than the CDF fit [Eq. (4); Figs. 4 and 5]. The CDF data also have the fewest fit parameters and there is no binning of the data.

Using any of the three methods to fit the distributions, we observe that the persistence length of high-salt microtubules is always about half as stiff as the control (Fig. 5, Table IV). Since the temperature is the same for all measurements, the change in the persistence length could be due to a change in the second moment of the area, I, and/or the Young's modulus, E [Eq. (1)].

We are interested in determining if the lattice structure of the high-salt microtubules has a different Young's elastic modulus

TABLE III. Cumulative probability distribution fits [Eq. (4)].

	μ	σ	R^2	L_p (mm)
Control	0.18 ± 0.02	0.79 ± 0.03	0.98	1.19 ± 0.04
High salt	-0.37 ± 0.01	0.72 ± 0.02	0.99	0.69 ± 0.02

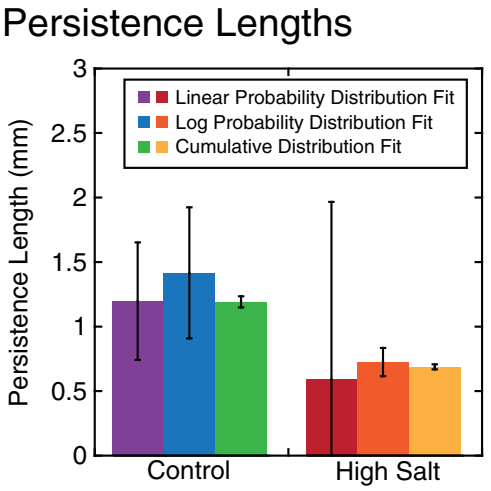

FIG. 5. Persistence length measurement and uncertainty depends on the method to create the distribution and the fit equation. Best fit for the characteristic persistence lengths of microtubules using the linear probability distribution fit to Eq. (2) (purple and red), using the Ln probability distribution fit to Eq. (3) (blue and orange), and using the cumulative distribution function fit to Eq. (4) (green and yellow).

than our typical control microtubules. Using Eq. (1), we can write an expression for the ratio of the Young's moduli for high-salt microtubules compared to control microtubules. This ratio depends on the ratio of the measured persistence lengths and the ratio of the second moments of area:

$$\frac{E_{\text{high salt}}}{E_{\text{control}}} = \frac{L_{p,\text{high salt}}}{L_{p,\text{control}}} \frac{I_{\text{control}}}{I_{\text{high salt}}}, \tag{5}$$

We can estimate the second moment of the area from models of microtubules with different protofilament numbers, from 13 to eight (Fig. 6). In these models, we approximated the protofilament as a perfect circle with a 4-nm cross-sectional diameter. These protofilaments were fit together to make a larger, hollow circle, which represented the microtubule cross section. The maximal inner and outer diameter of the microtubules were estimated from these models, and used to determine the second moment of area as given by

$$I = \frac{\pi}{4}\left(R_{\text{out}}^4 - R_{\text{in}}^4\right), \tag{6}$$

where R_{out} is the radius of the outer edge of the cylinder and R_{in} is the inner radius of the edge of the cylinder (Fig. 6).

Prior high-resolution electron microscopy on high-salt microtubules found that they had only about ten protofilaments [8,9] (Table IV, Fig. 6). Assuming that the high-salt microtubules are ten protofilaments and control microtubules are 12 protofilaments, the ratio of the second moments of the area would be 1.63.

Using the calculated values for the second moments of the area (Fig. 6), we can calculate the ratio of the Young's moduli

Protofilaments		R_{out}	R_{in}	$I = (\pi/4)(R_{out}^4 - R_{in}^4)$
13	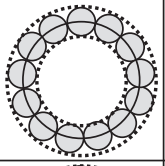	12.5 nm	7.5 nm	1.7×10^{-32} m^4
12	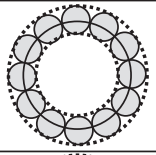	11.65 nm	6.85 nm	1.3×10^{-32} m^4
11	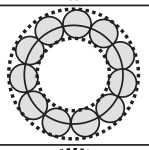	10.85 nm	6.05 nm	9.8×10^{-33} m^4
10	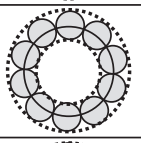	10.25 nm	5.4 nm	8.0×10^{-33} m^4
9		9.5 nm	4.72 nm	6.0×10^{-33} m^4
8	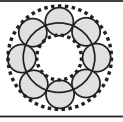	8.65 nm	3.75 nm	4.2×10^{-33} m^4

FIG. 6. Estimating the second moment of the area. Protofilaments (gray circles) are used to model the cross section of a microtubule with 13 to eight protofilaments. The largest outer and smallest inner diameters (dotted circles) were used to estimate the second moment of area. Prior EM studies show the number of protofilaments for *in vitro* microtubules vary from —eight to 15 protofilaments, while microtubules polymerized in the presence of high salt are —nine or ten protofilaments.

for the control and the high-salt microtubules: $E_{\text{high salt}}/E_{\text{control}}$ (Fig. 7). If the high-salt microtubules have eight protofilaments, and the control microtubules have 13 protofilaments, the elastic modulus of the high-salt microtubules would be greater than that of the control microtubules, suggesting that high-salt microtubules with more A lattice seams were stiffer than control microtubules (Fig. 7, upper left).

In regions where the high-salt microtubules are larger in radius, and the control microtubules are smaller (Fig. 7, lower right), the elastic modulus of the high-salt microtubules would be significantly lower than that of the control, suggesting that the seams could be weak points, as hypothesized by previous structural studies of microtubules.

TABLE IV. Persistence length, flexural rigidity, and estimated second moment of area of control and high salt microtubules.

	L_p (mm)	EI (Pa m^3)	I (estimated)	Protofilaments
Control	1.19 ± 0.04	$4.9 \pm 0.2 \times 10^{-24}$	1.3×10^{-32} m^4	12
High salt	0.69 ± 0.02	$2.83 \pm 0.08 \times 10^{-24}$	8.0×10^{-33} m^4	10

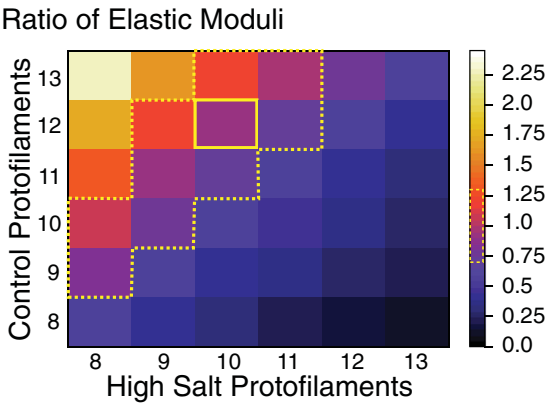

FIG. 7. Comparison of elastic moduli. The ratio of the elastic moduli for high-salt versus control microtubules depends on the ratios of the second moments of the area as given in Eq. (5). If high-salt microtubules are eight protofilaments and control microtubules are 13 protofilaments, the high-salt microtubules would be more rigid than control. If high-salt microtubules are equal in radius to the control microtubules, then the control microtubules are stiffer than high-salt microtubules. Given prior work from EM structural studies on high-salt and control microtubules, we would estimate that the high-salt microtubules are ten protofilaments and the control microtubules are 12 protofilaments (yellow box). In this case, the elastic moduli are equivalent.

Assuming that the high-salt microtubules are ten protofilaments and control microtubules are 12 protofilaments, as previously reported [8,9], the ratio of the Young's moduli would be 0.9 ± 0.3 (Fig. 7, yellow box). This number is not significantly different from unity, implying that the structure of the high-salt microtubules does not alter the elastic modulus of the microtubules. Further, we find there is a range of protofilament numbers where the elastic moduli of the high-salt microtubules are not distinguishable from those of the control microtubules (Fig. 7, dotted outlined region). Interestingly, the high-salt microtubules and the control microtubules have been previously shown to lie within this region—even when considering the distribution of protofilament numbers for a microtubule population [8]. Our results are consistent with a model that the persistence length decrease for high-salt microtubules is likely due to the change in cross-sectional radius, and not by the presence of the seam defects along the length of the high-salt microtubules.

IV. CONCLUSION

We present data on the bending stiffness of microtubules that have been polymerized in the presence of 580 m*M* NaCl and compare it to the stiffness of regular microtubules. Two prior *in vitro* studies showed that high-salt microtubules are predominantly 9or 10 protofilaments instead of the usual 11 or 12 protofilaments observed for microtubules polymerized from pure tubulin and stabilized with Taxol [8,9]. Such high-salt microtubules have also been shown to exhibit a high number of seam defects—where the lattice is a mix between A type and B type with equal probabilities [9]. The seams of the high-salt microtubules are the same as the single A lattice seam found in 13-protofilament cellular microtubules. The seam has long been speculated to be a weak point in the microtubule lattice because of its altered structure [5–7]. We show here, experimental evidence that the seam is not likely to be structurally weaker than the rest of the microtubule.

Our results show just how sensitive microtubule mechanics is to the cross-sectional radius of the microtubule. Although most microtubules are 13 protofilaments in cells, microtubules polymerized *in vitro* vary in protofilament number and are prone to lattice shift defects. Prior work has shown that polymerizing microtubules at a faster rate softens the microtubules; this is likely due to an increased number of protofilament shifts [18,21,29]. Given the prevalence of lattice defects *in vitro* and the high tubulin concentration, it is curious that cellular microtubules do not have lattice defects. Recent work has shown that microtubule associated proteins and enzymes likely work to inhibit or remove such defects including doublecortin [30] and katanin [31,32]. All the energy the cell spends to make perfect microtubules implies that the structure and perhaps the mechanical properties are crucial to correct cellular function.

In this study we used 580 m*M* NaCl to create structurally and mechanically altered microtubules. It would be interesting to further test the mechanical stiffness of microtubules with different types of salt ions at different valencies and various concentrations. Previously, it was shown that varying the ion concentration affects the polymerization rate of tubulin into microtubules [33]. Future work could determine if there is a correlation between the polymerization rate and the mechanical stiffness in the presence of different ions. Such studies would have broad implications to understanding how the microtubule structure impacts the mechanics of these important biopolymers.

ACKNOWLEDGMENTS

B.J.H., T.L.H., and J.L.R. were supported by NSF-DMR Grant No. 1207783 to J.L.R. T.L.H. was supported by NASA Training Grant No. NNX15AJ12H from the Wisconsin Space Consortium and UWL Faculty Research Grant to T.L.H. B.J.H. was supported by UWL Student and Faculty Research Grants to T.L.H.

[1] T. Müller-Reichert, D. Chrétien, F. Severin, and A. A. Hyman, Proc. Natl. Acad. Sci. USA **95**, 3661 (1998).
[2] L. A. Amos and A. Klug, J. Cell Sci. **14**, 523 (1974).
[3] M. Kikkawa, T. Ishikawa, T. Nakata, T. Wakabayashi, and N. Hirokawa, J. Cell Biol. **127**, 1965 (1994).
[4] R. W. Linck and G. L. Langevin, J. Cell Biol. **89**, 323 (1981).
[5] Q. Zhang, E. Fishel, T. Bertroche, and R. Dixit, Curr. Biol. **23**, 2191 (2013).
[6] G. M. Alushin, G. C. Lander, E. H. Kellogg, R. Zhang, D. Baker, and E. Nogales, Cell **157**, 1117 (2014).
[7] M. Katsuki, D. R. Drummond, and R. A. Cross, Nat. Commun. **5**, 3094 (2014).

[8] K. J. Böhm, W. Vater, P. Steinmetzer, and E. Unger, Acta Histochem. Suppl. **39**, 365 (1990).
[9] D. P. Dias and R. A. Milligan, J. Mol. Biol. **287**, 287 (1999).
[10] O. Kononova, Y. Kholodov, K. E. Theisen, K. A. Marx, R. I. Dima, F. I. Ataullakhanov, E. L. Grishchuk, and V. Barsegov, J. Am. Chem. Soc. **136**, 17036 (2014).
[11] D. Sept and F. C. MacKintosh, Phys. Rev. Lett. **104**, 018101 (2010).
[12] T. L. Hawkins, M. Mirigian, J. Li, M. S. Yasar, D. L. Sackett, D. Sept, and J. L. Ross, Cell. Mol. Bioeng. **5**, 227 (2012).
[13] T. L. Hawkins, D. Sept, B. Mogessie, A. Straube, and J. L. Ross, Biophys. J. **104**, 1517 (2013).
[14] F. Gittes, B. Mickey, J. Nettleton, and J. Howard, J. Cell. Biol. **120**, 923 (1993).
[15] A. Ott, M. Magnasco, A. Simon, and A. Libchaber, Phys. Rev. E **48**, R1642 (1993).
[16] C. P. Brangwynne, F. C. MacKintosh, S. Kumar, N. A. Geisse, J. Talbot, L. Mahadevan, K. K. Parker, D. E. Ingber, and D. A. Weitz, J. Cell Biol. **173**, 733 (2006).
[17] L. Cassimeris, D. Gard, P. T. Tran, and H. P. Erickson, J. Cell Sci. **114**, 3025 (2001).
[18] M. E. Janson and M. Dogterom, Biophys. J. **87**, 2723 (2004).
[19] K. Kawaguchi and A. Yamaguchi, Biochem. Biophys. Res. Commun. **402**, 66 (2010).
[20] B. Mickey and J. Howard, J. Cell Biol. **130**, 909 (1995).
[21] N. Isozaki, H. Shintaku, H. Kotera, T. L. Hawkins, J. L. Ross, and R. Yokokawa, Sci. Rob. **2**, eaan4882 (2017).
[22] B. J. Lopez and M. T. Valentine, Cytoskeleton **71**, 530 (2014).
[23] D. Valdman, P. J. Atzberger, D. Yu, S. Kuei, and M. T. Valentine, Biophys. J. **102**, 1144 (2012).
[24] J. Schindelin, I. Arganda-Carreras, E. Frise, V. Kaynig, M. Longair, T. Pietzsch, S. Preibisch, C. Rueden, S. Saalfeld, B. Schmid, J.-Y. Tinevez, D. J. White, V. Hartenstein, K. Eliceiri, P. Tomancak, and A. Cardona, Nat. Methods **9**, 676 (2012).
[25] R Development Code Team, *R: A Language and Environment for Statistical Computing* (R Foundation for Statistical Computing, Vienna, Austria, 2011).
[26] T. W. Kirkman, *Statistics to Use*, 1996. Available at http://www.physics.csbsju.edu/stats/.
[27] F. Pampaloni, G. Lattanzi, A. Jonáš, T. Surrey, E. Frey, and E.-L.-.L. Florin, Proc. Natl. Acad. Sci. USA **103**, 10248 (2006).
[28] D. Yu, V. Pessino, S. Kuei, and M. T. Valentine, Cytoskeleton **70**, 74 (2013).
[29] L. Schaedel, K. John, J. Gaillard, M. V. Nachury, L. Blanchoin, and M. Théry, Nat. Mater. **14**, 1156 (2015).
[30] S. Bechstedt and G. J. Brouhard, Dev. Cell. **23**, 181 (2012).
[31] L. J. Davis, D. J. Odde, S. M. Block, and S. P. Gross, Biophys. J. **82**, 2916 (2002).
[32] J. D. Díaz-Valencia, M. M. Morelli, M. Bailey, D. Zhang, D. J. Sharp, and J. L. Ross, Biophys. J. **100**, 2440 (2011).
[33] J. Wolff, D. L. Sackett, and L. Knipling, Protein Sci. **5**, 2020 (1996).